Synthetic Non-Abelian Gauge Fields for Non-Hermitian Systems

Zehai Pang,[1] Bengy Tsz Tsun Wong,[1] Jinbing Hu,[1,2] and Yi Yang[1,*]
[1]Department of Physics and HK Institute of Quantum Science and Technology, The University of Hong Kong, Pokfulam, Hong Kong, China
[2]College of Optical-Electrical Information and Computer Engineering, University of Shanghai for Science and Technology, Shanghai 200093, China

(Received 2 April 2023; accepted 27 November 2023; published 24 January 2024)

Non-Abelian gauge fields are versatile tools for synthesizing topological phenomena, but have so far been mostly studied in Hermitian systems, where gauge flux has to be defined from a closed loop in order for vector potentials, whether Abelian or non-Abelian, to become physically meaningful. We show that this condition can be relaxed in non-Hermitian systems by proposing and studying a generalized Hatano-Nelson model with imbalanced non-Abelian hopping. Despite lacking gauge flux in one dimension, non-Abelian gauge fields create rich non-Hermitian topological consequences. With SU(2) gauge fields, the braiding degrees that can be achieved are twice the highest hopping order of a lattice model, indicating the utility of spinful freedom to attain high-order nontrivial braiding. At both ends of an open chain, non-Abelian gauge fields lead to the simultaneous presence of non-Hermitian skin modes, whose population can be effectively tuned near the exceptional points. Generalizing to two dimensions, the gauge invariance of Wilson loops can also break down in non-Hermitian lattices dressed with non-Abelian gauge fields. Toward realization, we present a concrete experimental proposal for non-Abelian gauge fields in non-Hermitian systems via the synthetic frequency dimension of a polarization-multiplexed fiber ring resonator.

DOI: 10.1103/PhysRevLett.132.043804

Open physical systems coupled to external environments are described by non-Hermitian Hamiltonians that support complex eigenvalues. Compared to closed systems, non-Hermitian systems exhibit rich unique phenomena, such as power oscillations [1–3], unidirectional invisibility [3,4], and exceptional-point (EP) encirclement [5,6], which have no counterparts in Hermitian systems. In addition to their bulk invariants defined from eigenvectors [7–10] as in Hermitian systems, non-Hermitian systems also exhibit eigenvalue topology [11–21] due to the expansion of eigenenergies from the real to the complex regime. Importantly, non-Hermitian eigenstates of a nonvanishing eigenvalue winding number are all localized at the end of open systems, known as the non-Hermitian skin effect (NHSE) [7,10,21,22]. The NHSE has been implemented widely in photonics [18,23–26], acoustics [27–29], mechanics [30–32], and electric circuits [33–38]. Moreover, synthetic gauge fields have been introduced for better controlling non-Hermitian systems [39–44], but most efforts have been dedicated to Abelian gauge fields.

Non-Abelian physics has recently attracted a lot of attention in acoustics and photonics [45–66]. In particular, non-Abelian gauge fields, leveraging the internal degrees of freedom of particles, are a synthetic control knob for realizing non-Abelian physics in engineered physical systems [67]. These gauge fields enable synthetic spin-orbit interaction and can be used for creating non-Abelian Aharonov-Bohm interference and lattice models featuring complex gauge structures. Moreover, recent experiments have demonstrated the possibility of creating and tuning building blocks of non-Abelian gauge fields in fibers [47] and circuits [68], indicating their applicability for large lattice systems. The effectiveness of synthetic gauge fields substantially relies on their dimensionality. In particular, pure one-dimensional (1D) systems forbid the definition of closed loops and the associated magnetic flux. Thus, synthetic vector potentials, whether Abelian or non-Abelian, carry little physical consequences in 1D Hermitian systems. Although the 1D spin-orbit interaction realized with cold atoms [69] seems to be a counterexample, an extra Zeeman term has to be added for the Rashba-Dresselhaus gauge fields to become nontrivial. So far, non-Abelian gauge fields have seldom been explored in non-Hermitian systems, where the dimensionality constraint above could be violated.

The Hatano-Nelson model [70] is a prototypical 1D system that demonstrates the NHSE because of its nonreciprocal hoppings. We first extend the model with U(1) Abelian gauge fields as [Fig. 1(a)]

$$\hat{H}_0 = \sum_m J_{\mathrm{L}} \hat{c}_m^\dagger e^{i\theta_{\mathrm{L}}} \hat{c}_{m+1} + J_{\mathrm{R}} \hat{c}_{m+1}^\dagger e^{i\theta_{\mathrm{R}}} \hat{c}_m. \tag{1}$$

Here $\hat{c}_m^\dagger(\hat{c}_m)$ is the creation (annihilation) operator at site m, $J_{\mathrm{L(R)}}$ is the real hopping amplitude leftward (rightward), and $\theta_{\mathrm{L(R)}}$ are the corresponding hopping phases. The conventional Hatano-Nelson model is restored if $\theta_{\mathrm{L}} = \theta_{\mathrm{R}} = 0$. One can reformulate Eq. (1) as $H_0(k)e^{-i\theta_+} = J_{\mathrm{L}} e^{i(k+\theta_-)} + J_{\mathrm{R}} e^{-i(k+\theta_-)}$, where $\theta_+ = (\theta_{\mathrm{L}} + \theta_{\mathrm{R}})/2$ and $\theta_- = (\theta_{\mathrm{L}} - \theta_{\mathrm{R}})/2$. As in Hermitian systems, a Peierls substitution of θ_- acts on the momentum k. Meanwhile, on the left-hand side, a Peierls substitution of θ_+ acts on the complex energy, i.e., a

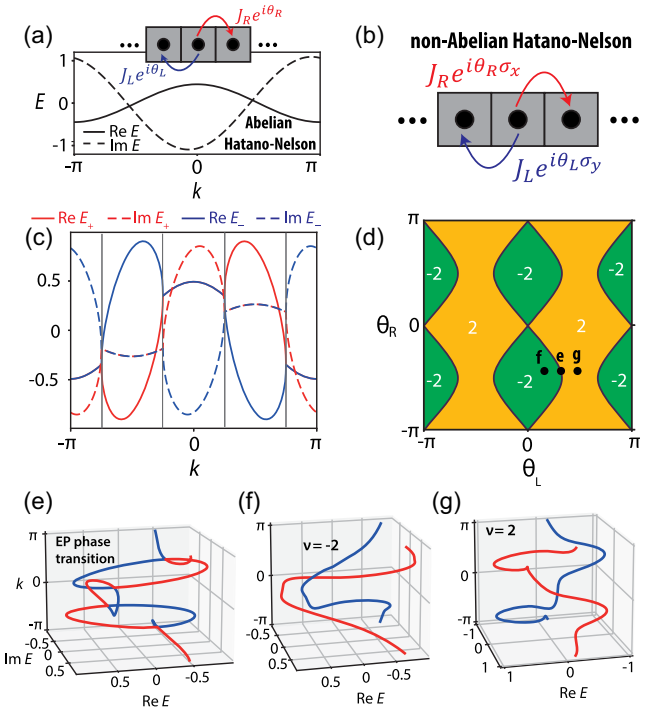

FIG. 1. Hatano-Nelson models with Abelian and non-Abelian gauge fields. (a) Hatano-Nelson model with nonreciprocal U(1) hopping phases and its single non-Hermitian band exhibiting a winding number $w = 1$. (b) Hatano-Nelson model with nonreciprocal SU(2) hopping phases. (c) Two non-Hermitian bands (E_+ and E_-) exhibiting four EPs at momenta $\{\pm\pi/4, \pm 3\pi/4\}$ (vertical gray lines). (d) Phase diagram of the non-Abelian Hatano-Nelson model under $J_L/J_R = 7/6$, featuring Hopf links with braid degrees $\nu = \pm 2$. Their phase transition accompanies the appearance of EPs (black solid lines). (e)–(g) Braiding of the two bands under the EP phase transition (e), $\nu = -2$ (f), and $\nu = 2$ (g) Hopf-link phases in the (ReE, ImE, k) space. Here we use $J_L = 0.7$, $J_R = 0.6$, and $\theta_R = -1.38$ throughout; $\theta_L = +1$ for (a), (c), and (e), $\theta_L = +0.5$ for (f), and $\theta_L = +1.5$ for (g), respectively, as shown by black dots in (d).

rotation on the complex energy plane. Thus, the U(1) fields only lead to trivial modifications to the Hatano-Nelson model. This is confirmed by the energy band shown in Fig. 1(a) that exhibits a winding number $w = +1$ on the complex energy plane, where $w \equiv (1/2\pi)\int_0^{2\pi} \partial_k \arg[E(k) - E_b]dk = \mathrm{sgn}(J_L - J_R)$, $E(k)$ is the periodic boundary condition (PBC) spectrum, and ± 1 indicates counterclockwise (CCW) and clockwise (CW) rotation, respectively, around a complex energy base point E_b inside the PBC spectrum on the complex plane [12].

In contrast, the model gets substantially modified with SU(2) non-Abelian gauge fields [Fig. 1(b)],

$$\hat{H} = \sum_m J_L \hat{c}_m^\dagger e^{i\theta_L \sigma_y} \hat{c}_{m+1} + J_R \hat{c}_{m+1}^\dagger e^{i\theta_R \sigma_x} \hat{c}_m, \quad (2)$$

where σ_x and σ_y are Pauli matrices. Notably, in Eq. (2), both the hopping amplitudes (J_L, J_R) and the non-Abelian hopping phases (θ_L, θ_R) contribute to non-Hermiticity. This feature distinguishes our system from a recent study on non-Hermitian Aubry-André-Harper models [71], where the non-Abelian on-site potentials alone do not cause non-Hermiticity. The Bloch Hamiltonian of Eq. (2) is

$$H(k) = A(k)\sigma_0 + iJ_L \sin\theta_L e^{ik}\sigma_y + iJ_R \sin\theta_R e^{-ik}\sigma_x, \quad (3)$$

where $A(k) = J_L \cos\theta_L e^{ik} + J_R \cos\theta_R e^{-ik}$ and σ_0 is the identity matrix. The eigenenergy of $\hat{H}$ is given by

$$E_\pm(k) = A(k) \pm i\sqrt{J_L^2 \sin^2\theta_L e^{i2k} + J_R^2 \sin^2\theta_R e^{-i2k}}. \quad (4)$$

Equation (4) permits EPs at $k_{EP} = \{\pm\pi/4, \pm 3\pi/4\}$ when

$$J_L^2 \sin^2\theta_L = J_R^2 \sin^2\theta_R \quad (5)$$

the EP condition is satisfied, as shown by an example spectrum in Fig. 1(c).

The two energy bands in Eq. (4) form the Hopf link in (ReE, ImE, k) space (different from the exceptional-line links in three-dimensional momentum space [72,73]). In fact, the EP condition Eq. (5) is the phase transition of the energy braiding between two types of Hopf links, defined by a braid degree $\nu = \pm 2$ [Fig. 1(d)], where

$$\nu \equiv \int_0^{2\pi} \frac{dk}{2\pi i} \frac{d}{dk} \ln \det\left(\hat{H}_k - \frac{1}{2}\mathrm{Tr}\hat{H}_k\right). \quad (6)$$

This braiding degree describes how many times the two bands braid in the $E - k$ space as k varies from 0 to 2π [18]. Figures 1(e)–1(g) confirm this transition, where Hopf links of opposite braiding degrees [Figs. 1(f) and 1(g)] appear on opposite sides of the EP phase transition [Fig. 1(e)]. Therefore, even though no gauge flux can be defined in a 1D bulk, introducing non-Abelian gauge fields can sufficiently drive non-Hermitian topological phase transitions, which is impossible for 1D Hermitian systems.

Non-Hermitian energy braiding of the Hopf-link type has been identified previously, but requires longer range hopping, such as the next-nearest-neighbor (NNN) coupling [18,19]. To see why the nearest-neighbor (NN) non-Abelian hopping here enables the Hopf braiding, consider a momentum-dependent gauge transformation $U = \mathrm{diag}(1, e^{ik})$. The non-Abelian model $H(k)$ [Eq. (3)] becomes $H'(k) = U^\dagger H(k) U$,

$$H'(k) = A(k)\sigma_0 + iJ_L \sin(\theta_L)\begin{pmatrix} 0 & -ie^{2ik} \\ i & 0 \end{pmatrix} + iJ_R \sin(\theta_R)\begin{pmatrix} 0 & 1 \\ e^{-2ik} & 0 \end{pmatrix}, \quad (7)$$

which maps the NN non-Abelian hopping to NN and NNN Abelian hoppings. Specifically, the blocks $(0, e^{\pm i2k}; 1, 0)$

were shown to enable a nontrivial Hopf braiding $\nu = \pm 2$ in Ref. [19]. Thus, the competition of the last two terms of Eq. (7) results in the dichotomy $\nu = \pm 2$ of the phase diagram, although the original $H(k)$ only features NN non-Abelian hopping. $H'(k)$ also fosters the understanding of the EP condition [Eq. (5)], under which a block in $H'(k)$ proportional to $(0, 1 \mp \mathrm{i}e^{2ik}; e^{-2ik} \pm \mathrm{i}, 0)$ appears, which is defective at $k = \pm\pi/4$ and $k = \pm 3\pi/4$. More generally, shown in Sec. S1 of the Supplemental Material [74], SU(2) non-Abelian gauge fields on the hopping order of n can realize a higher-order braid degree of $2n$, which reduces the hopping-order requirement for creating non-Hermitian topology via spinful particles.

Next, we show how non-Abelian gauge fields enrich the NHSE. Figure 2(a) shows the simultaneous presence of left-localized, right-localized, and extended eigenstates under the open boundary condition (OBC) of H, absent in the Abelian Hatano-Nelson model H_0 featured by U(1) gauge fields [see Eq. (1) and proof in Sec. S3.A [74]]. To explain this, we calculate the eigenspectra of H under PBC and OBC. The PBC spectra of H form closed loops surrounding the zero energy in the complex plane, indicating point-gapped bulk topology, while their OBC spectra become open arcs [15,77,78]. In particular, the PBC spectrum simultaneously exhibits CW and CCW winding at the four corners and center of the Hopf link, respectively. Consequently, the OBC arc enclosed by these sectors should demonstrate leftward [blue in Fig. 2(a)] and rightward [red in Fig. 2(a)] localization, respectively. Meanwhile, extended states [green in Fig. 2(a)] also appear at the boundary of the CW and CCW winding [green circles in Fig. 2(b)]. This simultaneous left- and rightward localization cannot be explained solely by the imbalanced hopping amplitudes $(J_\mathrm{L}, J_\mathrm{R})$. The analysis above is further confirmed by the non-Bloch [7,14,17] [Fig. 2(c)] and winding-number approaches [15], detailed in Secs. S3 and S4 of the Supplemental Material [74].

We specifically discuss the properties of zero modes $E = 0$ (details in Sec. S3 [74]) under OBC. All of the associated four non-Bloch solutions are $z = \pm\mathrm{i}\sqrt{J_\mathrm{R}/J_\mathrm{L}}e^{\pm\mathrm{i}\alpha}$, where $\alpha = \arctan(\sqrt{1-F^2}/F)$ and $F = \cos(\theta_\mathrm{R})\cos(\theta_\mathrm{L})$. All roots of the characteristic polynomial have equal absolute values, guaranteeing the existence of OBC zero modes, as can be seen by the pinned crossing at $E = 0$ in the complex plane [Fig. 2(b)]. We also prove that the OBC zero modes must be doubly degenerate (Sec. S3 [74]). Furthermore, The absolute values of the zero-mode non-Bloch solutions depend only on the ratio of the hopping amplitudes, which indicates that even SU(2) gauge fields cannot modify the localization direction of the zero modes (proof in Sec. S3 [74]).

Nevertheless, the localization of nonzero modes can be effectively manipulated by non-Abelian gauge fields. To further elucidate the interplay between the imbalanced

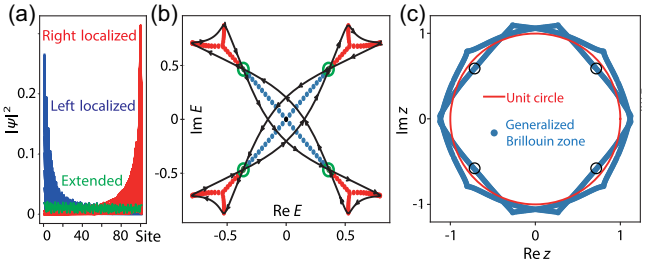

FIG. 2. Analysis of non-Hermitian skin effect. (a) Eigenstates under OBC of the non-Abelian Hatano-Nelson model. (b) Winding-number analysis: periodic- (black lines) and open-boundary (dots) spectra exhibit opposite winding depending on the choice of base energy E_b. Open-boundary eigenstates can be either extended (green), left-localized (blue), or right-localized (red). The black dot at the center denotes zero modes. (c) Non-Bloch analysis: the unit circle (red) intersects the generalized Brillouin zone (blue), indicating the simultaneous presence of left- (inside the unit circle) and right-localized (outside the unit circle) states. The black circles denote the zero-mode solutions. Here, $J_\mathrm{L} = 0.7$, $J_\mathrm{R} = 0.6$, $\theta_\mathrm{L} = -2.5$, $\theta_\mathrm{R} = -1.4$.

hopping amplitudes and non-Abelian gauge fields, we define a population contrast η in the OBC eigenstates as

$$\eta(J_\mathrm{L}, J_\mathrm{R}, \theta_\mathrm{L}, \theta_\mathrm{R}) \equiv (n_\mathrm{L} - n_\mathrm{R})/(n_\mathrm{L} + n_\mathrm{R} + n_\mathrm{E}), \quad (8)$$

where n_L, n_R, and n_E are the number of left- and right-localized and extended states, respectively. Figure 3 shows the population contrast as a function of the gauge fields $(\theta_\mathrm{L}, \theta_\mathrm{R})$ under different choices of $(J_\mathrm{L}, J_\mathrm{R})$.

Figure 3(a) exhibits an equal partition of the left and right localization under $J_\mathrm{L} = J_\mathrm{R}$, where non-Abelian gauge fields are the only origin of non-Hermiticity. η changes sign across the 45° and 135° lines defined by $\sin^2(\theta_\mathrm{L}) = \sin^2(\theta_\mathrm{R})$, exactly the EP phase transition condition. Notably, when $J_\mathrm{L} = J_\mathrm{R}$, the PBC spectrum collapses into an arc that overlaps with the OBC spectrum. Consequently, the winding number of all OBC energy points is zero, and all modes are extended. When $\theta_\mathrm{L} = \{0, \pm\pi\}$ or $\theta_\mathrm{R} = \{0, \pm\pi\}$, Eq. (4) reduces to the conventional Hatano-Nelson energy band under $J_\mathrm{L} = J_\mathrm{R}$, whose PBC spectrum also collapses into an arc and all OBC modes are extended; however, there is no phase transition there. In Figs. 3(b) and 3(c), as the imbalance between J_L and J_R appears and increases, localization tunability of the non-Abelian gauge fields becomes suppressed, as shown by the reduced red-colored area. Crucially, localization tuning is most effective (indicated by color variations in Fig. 3) near the EP phase transition [Eq. (5) and solid black lines in Fig. 3].

Asymptotic analysis (Sec. S5 [74]) reveals that the appearance of such tunability stems from the competition between the effective NNN hoppings [the last two terms in Eq. (7)]. Without loss of generality, we assume $J_\mathrm{L} > J_\mathrm{R}$ and obtain asymptotic expressions (details in Sec. S5) of

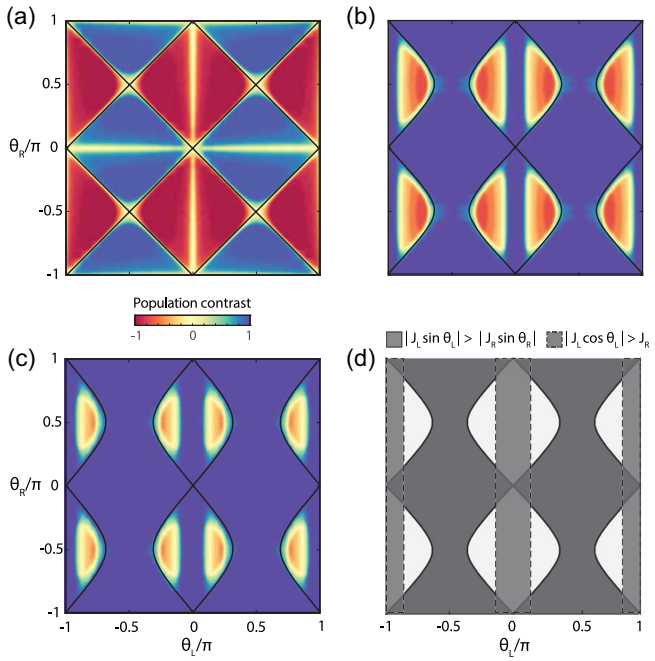

FIG. 3. Tuning non-Hermitian localization with non-Abelian gauge fields. (a)–(c) Population contrast η [Eq. (8)] in the (θ_L, θ_R) space when $(J_L, J_R) = (0.5, 0.5)$ (a), (0.55,0.5) (b), and (0.6,0.5) (c), respectively. The black solid lines define the exceptional-point phase boundary between the two braiding degrees $\nu = \pm 2$ [see Fig. 1(d)]. (d) Analytical asymptotic analysis. Effective high-order hoppings [Eqs. (9b) and (9c)] are non-negligible in the vicinity of the white region, where the localization tunability becomes most effective. In (d), we use $(J_L, J_R) = (0.55, 0.5)$, the same as those in (b).

both eigen-energies $E_\pm(k) \simeq$

$$J_L e^{\pm i\theta'_L} e^{ik} + J_R \cos\theta_R e^{-ik}, \quad \text{if } |J_L \sin\theta_L| \gg |J_R \sin\theta_R|, \tag{9a}$$

$$A(k) \pm iJ_L \left|\sin\theta_L\right| e^{ik} \sum_{n=0}^{\infty} C_n \left[\left(\frac{J_R \sin\theta_R}{J_L \sin\theta_L}\right)^2 e^{-i4k}\right]^n, \quad \text{if } |J_L \sin\theta_L| \gtrapprox |J_R \sin\theta_R|, \tag{9b}$$

$$A(k) \pm iJ_R \left|\sin\theta_R\right| e^{-ik} \sum_{n=0}^{\infty} C_n \left[\left(\frac{J_L \sin\theta_L}{J_R \sin\theta_R}\right)^2 e^{i4k}\right]^n, \quad \text{if } |J_L \sin\theta_L| \lessapprox |J_R \sin\theta_R|, \tag{9c}$$

$$J_L \cos\theta_L e^{ik} + J_R e^{\pm i\theta'_R} e^{-ik}, \quad \text{if } |J_L \sin\theta_L| \ll |J_R \sin\theta_R|, \tag{9d}$$

where $C_n = \frac{(-1)^{n-1}(2n)!}{4^n (n!)^2 (2n-1)}$ and $\theta'_{L/R} = \theta_{L/R} \mathrm{sgn}(\sin\theta_{L/R})$. Far away from the EP phase transition [Eqs. (9a) and (9d)], one NNN hopping dominates over the other [Eq. (7)], and the two eigenenergies are, respectively, governed by the Abelian Hatano-Nelson model under different hopping amplitudes—jointly forming a Hopf link. Specifically, a complete left localization is guaranteed for Eq. (9a) because $|J_L| > |J_R \cos\theta_R|$, while it additionally requires $|J_L \cos\theta_L| > |J_R|$ for Eq. (9d). Near the EP phase transition, both NNN couplings are non-negligible, resulting in the higher-order terms in Eqs. (9b) and (9c) that associate with the two braiding degrees, respectively. We plot in Fig. 3(d) two gray-shaded regions $|J_L \cos\theta_L| > |J_R| \cup |J_L \sin\theta_L| > |J_R \sin\theta_R|$. Their complementary parameter space is colored in white, near which non-negligible expansion terms occur. The analysis above indicates that the simultaneous presence of the NHSE on both ends of the open chain and the localization tunability should appear near the white region, as validated by the numerical calculation in Fig. 3(b).

Next, we present a concrete experimental proposal to realize non-Abelian gauge fields in non-Hermitian systems. We use polarization-maintaining fibers to form a ring resonator; its horizontal and vertical polarizations serve as the pseudospin [47], and its whispering gallery modes provide a synthetic frequency dimension [64,79]. From the target Hamiltonian [Eq. (2)], Floquet analysis (Sec. S6 [74]) enables the derivation of the single round-trip transfer matrix, comprising U(1) and SU(2) elements. The U(1) elements manipulate the two polarizations uniformly, while the SU(2) elements are constructed by spin rotation matrices ($U/U^\dagger$ or $V/V^\dagger$; can be realized with polarization rotators and phase retarders, see Sec. S6 in the Supplemental Material for the explicit form [74]) and the spin-dependent phase and amplitude modulation (along the σ_z axis) sandwiched between them. Concretely, the modulation signals for modulators 1–6 in Fig. 4(a) are given by $e^{-iT_R[J_L \cos(\theta_L) + J_R \cos(\theta_R)]\cos(\Omega_R t)}$, $e^{-iT_R \alpha \sin(\Omega_R t)}$, $e^{iT_R \alpha \sin(\Omega_R t)}$, $e^{T_R \alpha \cos(\Omega_R t)}$, $e^{-T_R \alpha \cos(\Omega_R t)}$, and $e^{T_R[-J_L \cos(\theta_L) + J_R \cos(\theta_R)]\sin(\Omega_R t)}$, respectively, where Ω_R is the free spectral range, $T_R = 2\pi/\Omega_R$ is the round-trip time, and $\alpha = \sqrt{[J_L \sin(\theta_L)]^2 + [J_R \sin(\theta_R)]^2}$ are constants associated with the modulation depths.

To extract the complex energy bands and their braiding, an input-output measurement [24,80] can be performed on the ring resonator. Continuous-wave laser light of arbitrary input polarization [via the polarizer and synthesizer in Fig. 4(a)] is injected into the ring resonator, with a tunable detuning $\delta\omega$ from a resonance frequency ω_n. We can measure the time (i.e., the quasimomentum k) and detuning-dependent projection detection of the transmission intensity in the linear basis [47], denoted as $I_h(k, \delta\omega)$ and $I_v(k, \delta\omega)$ for horizontal and vertical polarizations [Figs. 4(b) and 4(c)], respectively. The observables $I_h(k, \delta\omega)$ and $I_v(k, \delta\omega)$ can be used to extract the dispersion of both real and imaginary parts of the bands [e.g., Fig. 1(c)], as well as the braiding topology in the energy space [e.g., Figs. 1(e)–1(g)] via a fitting process (see details of the fitting in Sec. S8 [74]).

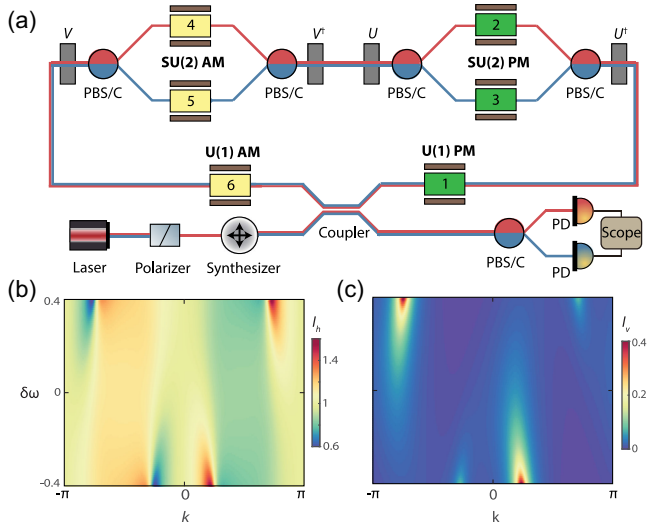

FIG. 4. Experimental proposal for non-Abelian gauge fields in non-Hermitian systems via the synthetic frequency dimension of a polarization-multiplexed fiber ring resonator. (a) Setup schematic. Optical elements are driven with appropriate modulation signals (detailed in the main text) to jointly realize a total of four functionalities, i.e., a U(1) phase modulation (PM), U(1) amplitude modulation (AM), SU(2) PM, and SU(2) AM, which jointly realize the non-Abelian Hatano-Nelson model. PBS/C, polarization beam splitter-combiner; PD, photodetector. (b),(c) Projection detection of the transmission spectra of horizontal and vertical polarizations, which can be used for extracting the complex energy to measure the Hopf braiding topology (see Supplemental Material Secs. S7 and S8 [74]). Here we use $J_L = 0.7$, $J_R = 0.3$, $\theta_L = 2$ rad, $\theta_R = -1$ rad with $|\psi_{\text{in}}\rangle = (1, 0)^T$.

Finally, we generalize our discussions to 2D non-Hermitian lattices, where the gauge invariance of the Wilson loop could break down in non-Abelian gauge fields. The Wilson loop is a foundational quantity for studying the behavior of gauge fields in lattice models [81]. It is defined as the trace of the loop operator, i.e., the path-ordered product of link variables around a closed loop [45]. The loop operators of a given plaquette are nonunique (e.g., along the CW and CCW directions) but unitary transformation partners in Hermitian systems, leading to the gauge-invariant property of Wilson loops (see detailed discussions and examples in Sec. S9 [74]).

To see how the gauge invariance of the Wilson loop gets modified, we further generalize the 1D non-Abelian Hatano-Nelson model to 2D,

$$\hat{H}_{2D} = \sum_{m,n} J_U \hat{c}^\dagger_{m,n+1} e^{i\theta_U \sigma_z} \hat{c}_{m,n} + J_D \hat{c}^\dagger_{m,n} e^{i\theta_D \sigma_0} \hat{c}_{m,n+1} + J_R \hat{c}^\dagger_{m+1,n} e^{i\theta_R \sigma_x} \hat{c}_{m,n} + J_L \hat{c}^\dagger_{m,n} e^{i\theta_L \sigma_y} \hat{c}_{m+1,n}. \quad (10)$$

This model features hopping phases $\theta_L \sigma_y$, $\theta_R \sigma_x$, $\theta_U \sigma_z$, and $\theta_D \sigma_0$ for left-, right-, up-, and downward, respectively. We further assume that the hopping amplitudes are all equal $J_L = J_R = J_U = J_D$ such that the non-Hermiticity solely stems from the non-Abelian hopping phases. The Wilson loops $W^{\text{NH}}_{\text{cw,ccw}}$ of the CW and CCW loop operators [Fig. 5(a) bottom] are

$$W^{\text{NH}}_{\text{cw,ccw}} = 2e^{i\theta_D}[\cos(\theta_U)\cos(\theta_L)\cos(\theta_R) \pm \sin(\theta_U)\sin(\theta_L)\sin(\theta_R)], \quad (11)$$

where $+$ is for CW, $-$ is for CCW, and the superscript NH stands for "non-Hermitian." Evidently, the CW and CCW Wilson loops now differ; this calls for further study of non-Abelian magnetic fields in non-Hermitian systems, which could lead to intriguing dynamics.

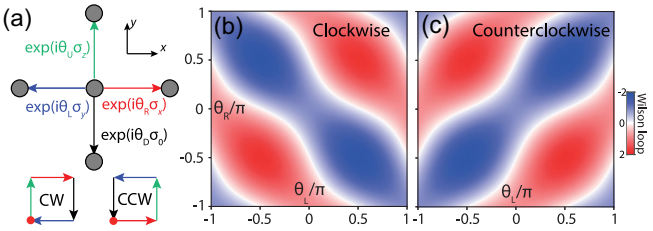

FIG. 5. Distinct Wilson loops for the same plaquette in a non-Hermitian non-Abelian lattice model. (a) A 2D square-lattice model featuring hopping phases $\theta_L \sigma_y$, $\theta_R \sigma_x$, $\theta_U \sigma_z$, and $\theta_D \sigma_0$ for left-, right-, up-, and downward, respectively. Loop operators along the CW and CCW directions can be defined. The red point indicates the starting point of the Wilson loop. (b),(c) Distinct CW and CCW Wilson loop for a single plaquette in the (θ_L, θ_R) parameter space. Here we fix $\theta_U = 2$, $\theta_D = 0$.

In conclusion, we introduce and study non-Abelian gauge fields as an origin of non-Hermiticity. Non-Abelian gauge fields enable non-Hermitian topological phase transition and tunable NHSE despite the lack of gauge flux in one dimension. The presence of the spinful freedom expands the achievable range of braiding degrees under a given maximal hopping order. In 2D non-Hermitian lattices, non-Abelian gauge fields further disrupt the gauge invariance of the Wilson loop. A concrete experimental scheme has been proposed to realize the non-Abelian Hatano-Nelson model in the synthetic frequency dimension of a polarization-multiplexed ring resonator. The findings presented here could offer unexplored avenues in non-Hermitian topology via synthetic non-Abelian gauge fields.

The authors thank the reviewer for introducing the gauge transformation in Eq. (7). The authors acknowledge the support from the National Natural Science Foundation of China Excellent Young Scientists Fund (HKU 12222417), the Hong Kong Research Grant Council Strategic Topics Grant No. STG3/E-704/23-N, the startup fund of The University of Hong Kong, and the Asian Young Scientist Fellowship.

*yiyg@hku.hk

[1] Z. H. Musslimani, K. G. Makris, R. El-Ganainy, and D. N. Christodoulides, Phys. Rev. Lett. **100**, 030402 (2008).

[2] K. G. Makris, R. El-Ganainy, D. N. Christodoulides, and Z. H. Musslimani, Phys. Rev. Lett. **100**, 103904 (2008).
[3] A. Regensburger, C. Bersch, M.-A. Miri, G. Onishchukov, D. N. Christodoulides, and U. Peschel, Nature (London) **488**, 167 (2012).
[4] L. Feng, Y.-L. Xu, W. S. Fegadolli, M.-H. Lu, J. E. Oliveira, V. R. Almeida, Y.-F. Chen, and A. Scherer, Nat. Mater. **12**, 108 (2013).
[5] T. Gao, E. Estrecho, K. Bliokh, T. Liew, M. Fraser, S. Brodbeck, M. Kamp, C. Schneider, S. Höfling, Y. Yamamoto *et al.*, Nature (London) **526**, 554 (2015).
[6] J. Doppler, A. A. Mailybaev, J. Böhm, U. Kuhl, A. Girschik, F. Libisch, T. J. Milburn, P. Rabl, N. Moiseyev, and S. Rotter, Nature (London) **537**, 76 (2016).
[7] S. Yao and Z. Wang, Phys. Rev. Lett. **121**, 086803 (2018).
[8] F. Song, S. Yao, and Z. Wang, Phys. Rev. Lett. **123**, 246801 (2019).
[9] F. K. Kunst, E. Edvardsson, J. C. Budich, and E. J. Bergholtz, Phys. Rev. Lett. **121**, 026808 (2018).
[10] Y. Xiong, J. Phys. Commun. **2**, 035043 (2018).
[11] E. J. Bergholtz, J. C. Budich, and F. K. Kunst, Rev. Mod. Phys. **93**, 015005 (2021).
[12] Z. Gong, Y. Ashida, K. Kawabata, K. Takasan, S. Higashikawa, and M. Ueda, Phys. Rev. X **8**, 031079 (2018).
[13] K. Kawabata, K. Shiozaki, M. Ueda, and M. Sato, Phys. Rev. X **9**, 041015 (2019).
[14] K. Yokomizo and S. Murakami, Phys. Rev. Lett. **123**, 066404 (2019).
[15] K. Zhang, Z. Yang, and C. Fang, Phys. Rev. Lett. **125**, 126402 (2020).
[16] N. Okuma, K. Kawabata, K. Shiozaki, and M. Sato, Phys. Rev. Lett. **124**, 086801 (2020).
[17] Z. Yang, K. Zhang, C. Fang, and J. Hu, Phys. Rev. Lett. **125**, 226402 (2020).
[18] K. Wang, A. Dutt, C. C. Wojcik, and S. Fan, Nature (London) **598**, 59 (2021).
[19] H. Hu and E. Zhao, Phys. Rev. Lett. **126**, 010401 (2021).
[20] D. S. Borgnia, A. J. Kruchkov, and R.-J. Slager, Phys. Rev. Lett. **124**, 056802 (2020).
[21] K. Ding, C. Fang, and G. Ma, Nat. Rev. Phys. **4**, 745 (2022).
[22] T. E. Lee, Phys. Rev. Lett. **116**, 133903 (2016).
[23] S. Weidemann, M. Kremer, T. Helbig, T. Hofmann, A. Stegmaier, M. Greiter, R. Thomale, and A. Szameit, Science **368**, 311 (2020).
[24] K. Wang, A. Dutt, K. Y. Yang, C. C. Wojcik, J. Vučković, and S. Fan, Science **371**, 1240 (2021).
[25] L. Xiao, T. Deng, K. Wang, G. Zhu, Z. Wang, W. Yi, and P. Xue, Nat. Phys. **16**, 761 (2020).
[26] Y. G. Liu, Y. Wei, O. Hemmatyar, G. G. Pyrialakos, P. S. Jung, D. N. Christodoulides, and M. Khajavikhan, Light **11**, 336 (2022).
[27] X. Zhang, Y. Tian, J.-H. Jiang, M.-H. Lu, and Y.-F. Chen, Nat. Commun. **12**, 5377 (2021).
[28] L. Zhang, Y. Yang, Y. Ge, Y.-J. Guan, Q. Chen, Q. Yan, F. Chen, R. Xi, Y. Li, D. Jia *et al.*, Nat. Commun. **12**, 6297 (2021).
[29] Z. Gu, H. Gao, H. Xue, J. Li, Z. Su, and J. Zhu, Nat. Commun. **13**, 7668 (2022).
[30] W. Wang, X. Wang, and G. Ma, Nature (London) **608**, 50 (2022).
[31] A. Ghatak, M. Brandenbourger, J. Van Wezel, and C. Coulais, Proc. Natl. Acad. Sci. U.S.A. **117**, 29561 (2020).
[32] C. Scheibner, W. T. M. Irvine, and V. Vitelli, Phys. Rev. Lett. **125**, 118001 (2020).
[33] L. Li, C. H. Lee, S. Mu, and J. Gong, Nat. Commun. **11**, 5491 (2020).
[34] T. Helbig, T. Hofmann, S. Imhof, M. Abdelghany, T. Kiessling, L. Molenkamp, C. Lee, A. Szameit, M. Greiter, and R. Thomale, Nat. Phys. **16**, 747 (2020).
[35] T. Hofmann, T. Helbig, F. Schindler, N. Salgo, M. Brzezińska, M. Greiter, T. Kiessling, D. Wolf, A. Vollhardt, A. Kabaši *et al.*, Phys. Rev. Res. **2**, 023265 (2020).
[36] S. Liu, R. Shao, S. Ma, L. Zhang, O. You, H. Wu, Y. J. Xiang, T. J. Cui, and S. Zhang, Research **2021**, 5608038 (2021).
[37] D. Zou, T. Chen, W. He, J. Bao, C. H. Lee, H. Sun, and X. Zhang, Nat. Commun. **12**, 7201 (2021).
[38] C. Shang, S. Liu, R. Shao, P. Han, X. Zang, X. Zhang, K. N. Salama, W. Gao, C. H. Lee, R. Thomale *et al.*, Adv. Sci. **9**, 2202922 (2022).
[39] Z. Lin, L. Ding, S. Ke, and X. Li, Opt. Lett. **46**, 3512 (2021).
[40] B. Midya, H. Zhao, and L. Feng, Nat. Commun. **9**, 2674 (2018).
[41] S. Longhi, Phys. Rev. B **95**, 014201 (2017).
[42] S. Longhi, D. Gatti, and G. Della Valle, Phys. Rev. B **92**, 094204 (2015).
[43] S. Longhi, Phys. Rev. A **95**, 062122 (2017).
[44] S. Wong and S. S. Oh, Phys. Rev. Res. **3**, 033042 (2021).
[45] Y. Yang, B. Yang, G. Ma, J. Li, S. Zhang, and C. Chan, arXiv:2305.12206.
[46] Y. Chen, R.-Y. Zhang, Z. Xiong, Z. H. Hang, J. Li, J. Q. Shen, and C. T. Chan, Nat. Commun. **10**, 1 (2019).
[47] Y. Yang, C. Peng, D. Zhu, H. Buljan, J. D. Joannopoulos, B. Zhen, and M. Soljačić, Science **365**, 1021 (2019).
[48] E. Yang, B. Yang, O. You, H.-C. Chan, P. Mao, Q. Guo, S. Ma, L. Xia, D. Fan, Y. Xiang *et al.*, Phys. Rev. Lett. **125**, 033901 (2020).
[49] Q. Guo, T. Jiang, R.-Y. Zhang, L. Zhang, Z.-Q. Zhang, B. Yang, S. Zhang, and C. T. Chan, Nature (London) **594**, 195 (2021).
[50] B. Jiang, A. Bouhon, Z.-K. Lin, X. Zhou, B. Hou, F. Li, R.-J. Slager, and J.-H. Jiang, Nat. Phys. **17**, 1239 (2021).
[51] V. Brosco, L. Pilozzi, R. Fazio, and C. Conti, Phys. Rev. A **103**, 063518 (2021).
[52] Z.-G. Chen, R.-Y. Zhang, C. T. Chan, and G. Ma, Nat. Phys. **18**, 179 (2022).
[53] Y.-K. Sun, X.-L. Zhang, F. Yu, Z.-N. Tian, Q.-D. Chen, and H.-B. Sun, Nat. Phys. **18**, 1080 (2022).
[54] O. You, S. Liang, B. Xie, W. Gao, W. Ye, J. Zhu, and S. Zhang, Phys. Rev. Lett. **128**, 244302 (2022).
[55] J. Noh, T. Schuster, T. Iadecola, S. Huang, M. Wang, K. P. Chen, C. Chamon, and M. C. Rechtsman, Nat. Phys. **16**, 989 (2020).
[56] X.-L. Zhang, F. Yu, Z.-G. Chen, Z.-N. Tian, Q.-D. Chen, H.-B. Sun, and G. Ma, Nat. Photonics **16**, 390 (2022).
[57] J.-S. Xu, K. Sun, Y.-J. Han, C.-F. Li, J. K. Pachos, and G.-C. Guo, Nat. Commun. **7**, 13194 (2016).

[58] Y. Yang, B. Zhen, J. D. Joannopoulos, and M. Soljačić, Light **9**, 177 (2020).
[59] Y. Yang, H. C. Po, V. Liu, J. D. Joannopoulos, L. Fu, and M. Soljačić, Phys. Rev. B **106**, L161108 (2022).
[60] A. Gianfrate, O. Bleu, L. Dominici, V. Ardizzone, M. De Giorgi, D. Ballarini, G. Lerario, K. W. West, L. N. Pfeiffer, D. D. Solnyshkov, D. Sanvitto, and G. Malpuech, Nature (London) **578**, 381 (2020).
[61] C. Whittaker, T. Dowling, A. Nalitov, A. Yulin, B. Royall, E. Clarke, M. Skolnick, I. Shelykh, and D. Krizhanovskii, Nat. Photonics **15**, 193 (2021).
[62] T. Iadecola, T. Schuster, and C. Chamon, Phys. Rev. Lett. **117**, 073901 (2016).
[63] L. Polimeno, A. Fieramosca, G. Lerario, L. De Marco, M. De Giorgi, D. Ballarini, L. Dominici, V. Ardizzone, M. Pugliese, C. Prontera *et al.*, Optica **8**, 1442 (2021).
[64] D. Cheng, K. Wang, and S. Fan, Phys. Rev. Lett. **130**, 083601 (2023).
[65] A. Bouhon, Q. Wu, R.-J. Slager, H. Weng, O. V. Yazyev, and T. Bzdušek, Nat. Phys. **16**, 1137 (2020).
[66] B. Jiang, A. Bouhon, S.-Q. Wu, Z.-L. Kong, Z.-K. Lin, R.-J. Slager, and J.-H. Jiang, arXiv:2205.03429.
[67] M. Aidelsburger, S. Nascimbene, and N. Goldman, C.R. Phys. **19**, 394 (2018).
[68] J. Wu, Z. Wang, Y. Biao, F. Fei, S. Zhang, Z. Yin, Y. Hu, Z. Song, T. Wu, F. Song *et al.*, Nat. Electron. **5**, 635 (2022).
[69] Y.-J. Lin, K. Jiménez-García, and I. B. Spielman, Nature (London) **471**, 83 (2011).
[70] N. Hatano and D. R. Nelson, Phys. Rev. Lett. **77**, 570 (1996).
[71] L. Zhou, Phys. Rev. B **108**, 014202 (2023).
[72] Z. Yang and J. Hu, Phys. Rev. B **99**, 081102(R) (2019).
[73] J. Carlström and E. J. Bergholtz, Phys. Rev. A **98**, 042114 (2018).
[74] See Supplemental Material at http://link.aps.org/supplemental/10.1103/PhysRevLett.132.043804 for additional notes on (i) non-Abelian gauge fields in higher-order hopping, (ii) Hopf link, (iii) non-Bloch approach, (iv) winding-number approach, (v) asymptotic analysis, (vi) detailed experimental proposal, which includes Ref. [75], (vii) projection detection, (viii) spectral fitting, and (ix) breakdown of gauge-invariant Wilson loops in non-Hermitian systems, which includes Ref. [76].
[75] L. Yuan and S. Fan, Optica **3**, 1014 (2016).
[76] N. Goldman, A. Kubasiak, P. Gaspard, and M. Lewenstein, Phys. Rev. A **79**, 023624 (2009).
[77] X. Zhang, T. Zhang, M.-H. Lu, and Y.-F. Chen, Adv. Phys. **7**, 2109431 (2022).
[78] Y. Ashida, Z. Gong, and M. Ueda, Adv. Phys. **69**, 249 (2020).
[79] L. Yuan, Q. Lin, M. Xiao, and S. Fan, Optica **5**, 1396 (2018).
[80] A. Dutt, M. Minkov, Q. Lin, L. Yuan, D. A. Miller, and S. Fan, Nat. Commun. **10**, 3122 (2019).
[81] K. G. Wilson, Phys. Rev. D **10**, 2445 (1974).